Biophysical *Journal*
Article

Biophysical Society

Different Vinculin Binding Sites Use the Same Mechanism to Regulate Directional Force Transduction

Carleen Kluger,[1] Lukas Braun,[2] Steffen M. Sedlak,[1] Diana A. Pippig,[1] Magnus S. Bauer,[1] Ken Miller,[1] Lukas F. Milles,[1] Hermann E. Gaub,[1] and Viola Vogel[2,*]
[1]Lehrstuhl für Angewandte Physik and Center for NanoScience, Ludwig-Maximilians-Universität München, Munich, Germany and [2]Laboratory of Applied Mechanobiology, Department of Health Sciences and Technology, ETH Zurich, Zurich, Switzerland

ABSTRACT Vinculin is a universal adaptor protein that transiently reinforces the mechanical stability of adhesion complexes. It stabilizes mechanical connections that cells establish between the actomyosin cytoskeleton and the extracellular matrix via integrins or to neighboring cells via cadherins, yet little is known regarding its mechanical design. Vinculin binding sites (VBSs) from different nonhomologous actin-binding proteins use conserved helical motifs to associate with the vinculin head domain. We studied the mechanical stability of such complexes by pulling VBS peptides derived from talin, α-actinin, and *Shigella* IpaA out of the vinculin head domain. Experimental data from atomic force microscopy single-molecule force spectroscopy and steered molecular dynamics (SMD) simulations both revealed greater mechanical stability of the complex for shear-like than for zipper-like pulling configurations. This suggests that reinforcement occurs along preferential force directions, thus stabilizing those cytoskeletal filament architectures that result in shear-like pulling geometries. Large force-induced conformational changes in the vinculin head domain, as well as protein-specific fine-tuning of the VBS sequence, including sequence inversion, allow for an even more nuanced force response.

SIGNIFICANCE The cytoskeleton is known to realign along major force-bearing cell axes, which increases cell contractility. Our data suggest not only that vinculin transiently reinforces critical linkages of the cytoskeleton to various adhesion hub proteins, as previously thought, but also that the geometry by which the forces are applied to the vinculin complexes tunes the mechanical stability such that shear-like pulling geometries outcompete other interactions. By acting as a mechanosensitive logical gate that converts the inputs force, geometry, and magnitude into distinct structural outputs with potentially different biological functions.

INTRODUCTION

Wherever cells form force-bearing connections between the actin cytoskeleton and their extracellular surroundings, the adaptor protein vinculin is present (Fig. 1 *A*; (1,2)). This includes structures like focal adhesions, filopodia, adherens junctions, and immunological synapses (3–8). Although vinculin acts as a signaling hub with a multitude of binding partners, it is best known for its ability to physically reinforce the connections between actin filaments and adhesion proteins like talin, α-actinin, or α-catenin (2). All of these proteins contain vinculin binding sites (VBSs) that are hidden inside mechanically labile helix bundles and are exposed upon force-induced unfolding (Fig. 1 *B*; (9–13)).

Remarkably, vinculin uses the same structural mechanism to bind multiple nonhomologous adhesion proteins, which contain either one (e.g., α-actinin, α-catenin) or up to 11 helical VBSs (e.g., talin) (14–16). In addition, some pathogenic bacteria, like *Shigella*, have evolved invasion proteins that mimic VBSs to hijack the contractile machinery and enter into the host cell (Fig. 1 *A*; (17)). So far, more than 70 confirmed and putative VBSs of different affinity have been described and can be aligned to a consensus sequence, as shown in Table S1 (15). X-ray crystallography revealed that the first domain of vinculin head (Vd1) binds

Submitted July 25, 2019, and accepted for publication December 30, 2019.
*Correspondence: viola.vogel@hest.ethz.ch
Carleen Kluger and Lukas Braun contributed equally to this work.
Diana A. Pippig's present address is Roche Innovation Center Munich, Nonnewald 2, 82377 Penzberg, Germany.
Editor: Alexander Dunn.
https://doi.org/10.1016/j.bpj.2019.12.042

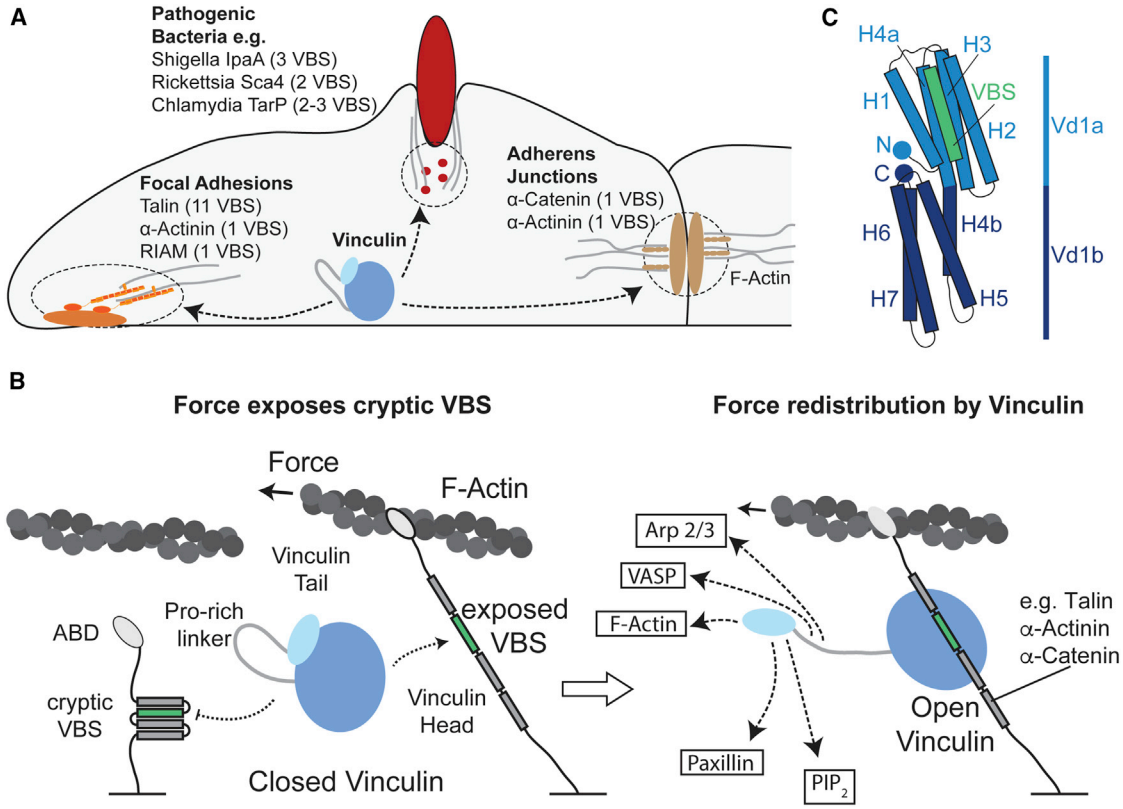

FIGURE 1 Interaction of vinculin with vinculin binding sites (VBS) in different adhesion structures. (*A*) Vinculin can be recruited to multiple proteins in cellular structures, which are associated with adhesions or the cytoskeleton. (*B*) VBS of proteins like talin, α-actinin, or α-catenin are not accessible when their ABD is not engaged to the F-actin cytoskeleton. F-Actin binding and force-induced unfolding of helical domains exposes the VBS. VBS binding activates vinculin by triggering the release of its head from the tail domain. The free vinculin tail can then either engage with the F-actin cytoskeleton or bind to PIP_2-enriched membranes. Thus, a multitude of relative pulling directions between strain gauge proteins and vinculin are possible. (*C*) Vinculin head domain 1 (Vd1) consists of seven α-helices arranged in two four-helix bundles (Vd1a and Vd1b) with a shared long helix (H4). VBSs are short (20–24 aa) α-helical peptides, which insert into upper subdomain Vd1a in a mechanism called helical bundle conversion. To see this figure in color, go online.

to these VBSs using a mechanism termed helical bundle conversion (14). Insertion of the amphipathic VBS helix into the N-terminal part of Vd1 converts it from a monomeric four-helix to a heterodimeric five-helix bundle (Fig. 1 *C*). It has been shown that differences in the VBS sequence tune affinity to vinculin and can also influence the mechanical stability of the helical bundles in which they reside (18). However, it is not clear whether and how strongly the mechanical stability of the vinculin-VBS connection itself can be tuned by VBS sequence.

By use of molecular tension sensors, it has been demonstrated that piconewton (pN) mechanical forces are transmitted across focal adhesion components like vinculin and VBS-containing proteins such as talin or α-actinin (19–22). However, tension sensors are not able to resolve molecular details of force transmission and only report average force over a large ensemble of molecules. Because both vinculin and the VBS-containing proteins possess actin binding domains (ABDs), it is possible that they interact with F-actin filaments of different relative orientations. Furthermore, they are subjected to interactions with additional binding partners, including paxillin, VASP, Arp2/3, or components of the plasma membrane, like phosphatidylinositol 4,5-bisphosphate (Fig. 1 *B*; (2)). This gives rise to a multitude of different force loading directions of vinculin relative to the VBSs (Fig. 1 *B*). Although exposure of cryptic VBSs has been studied in detail, little is known about the mechanical stability of the vinculin-VBS complex, and even less is known about how it might be influenced by pulling geometry.

The strongest hint that the direction of force transduction across the vinculin-VBS complex plays an important role is suggested by its binding to talin versus α-actinin: in contrast to all other VBSs, the VBS of α-actinin only matches the consensus sequence when it is read in the reverse direction. X-ray crystallography confirmed that the C- and N-termini are indeed inverted in the crystal structure (16). This reversal in VBS binding site orientation comes along with an inverted domain organization: although the other VBS-containing proteins are anchored at their N-terminus (FERM domain in talin, N-domain in α-catenin) and bind to F-actin with their C-terminus (23,24), α-actinin has an

N-terminal ABD, and its C-terminal EF-hand domains are putative anchor points (11). The flipped VBS polarity allows vinculin to assume the same orientation relative to the anchor point and the ABD, suggesting that there is high selection pressure on maintaining this configuration and, thus, a defined force transduction pathway.

This directly leads to the question of whether VBS orientation indeed causes differences in force transduction across the vinculin-VBS complex.

Thus, to probe the mechanical response of the vinculin-VBS complex, we combined data from single-molecule force spectroscopy (SMFS) measurements performed with the atomic force microscopy (AFM) and all-atom steered molecular dynamics (SMD) simulations. The setups for experiment and simulations are designed to be as similar as possible: in both cases, the first vinculin head domain is fixed at its C-terminus and binds to VBS peptides, which are pulled at a constant velocity either via their N- or C-terminus. For each VBS, this results in two different pulling geometries (Fig. 1 *D*). Thus, we can compare the forces at which the vinculin-VBS complex ruptures when it is subjected to mechanical force in two different directions. Together, the different time- and length-scales of experiment and simulation enable us to determine the molecular mechanisms that underlie the rupture of the complex.

MATERIALS AND METHODS

Selecting VBS from talin, *Shigella* IpaA, and α-actinin for detailed analysis

To gain a better overview of VBS sequences, we aligned 75 different VBSs from nine different proteins, which have been reported in the literature (Table S1). We chose talin VBS58 (talin residues 2345–2369, Talin Gene Bank: AAF23322.1) for our analysis, which had shown a strong interaction in a SPOT-peptide assay (15) and is located in the highly conserved part of the C-terminal I/LWEQ or THATCH region of talin (25). Talin VBS58 is located in the atypical 5-helix bundle R13, which can bind actin. However, it remains under discussion whether this VBS is actually involved in vinculin binding in vivo (26). Talin VBS11 (talin residues 820–843) is located in the third rod bundle (R3) (27), which is a structurally labile 4-helix bundle and thus is likely to unfold early after the onset of force application to talin (28). R13 and R3 are located on opposite ends of the talin rod and therefore belong to different focal adhesion (FA) layers. Although R13 mostly resides in the force transducing layer and actin regulatory layer (29,30), R3 is in close proximity to the cell membrane. This exposes them to a different pool of interaction partners. Among the various bacterial interactors of vinculin, we decided for a binding site of the *Shigella* invasin IpaA (VBSIpaA1: IpaA residues 611–632), for which high affinity to both full-length vinculin and the first vinculin head domain has been reported (17). Recently, the dual role of IpaA VBS3 as a talin and vinculin binding site was described, opening up new possible mechanisms of linking talin and vinculin via IpaA (31). Instead of only activating vinculin or blocking Vd1 interaction with talin, IpaA could also have a role in mechanotransduction by modulating the relative pulling directions of talin and vinculin. In comparison with all other VBSs, the VBS of α-actinin (VBSαAct: α-actinin residues 741–764) binds the Vd1 helix bundle in an inverted orientation. This makes it an interesting target to understand the directional dependence of VBS-Vd1 interaction.

Generation of proteins and design of peptides

To generate constructs of Vd1, the first 258 amino acids (aa) of vinculin were cloned into pET28 vectors (Novagen, EMD Millipore, Billerica) containing an N-terminal polyhistidine tag (6xHis) and a PreScission (PreSc) cleavage site using standard restriction enzyme cloning. Vd1 domain was flanked by StrepTag II (SII, WSHPQFEK) and ybbR tag (DSLEFIASKLA) at the opposite ends in both orientations (ybbR–Vd1–SII, SII–Vd1-ybbR). To ensure flexibility, 4-aa GSGS linkers were inserted between domain and tags. For full sequences, please refer to the Supporting Material. For VBS constructs used in isothermal titration calorimetry (ITC) and Native polyacrylamide gel electrophoresis, DNA oligonucleotides of around 100–120 basepairs including the VBS sequence and suitable restriction enzyme cutting sites (NheI/XhoI for N-terminal ybbR tag) were purchased (MWG Eurofins, Ebersberg, Germany). DNA strands of two opposing directions were heated up to 95°C for 5 min and cooled down to room temperature before being cut with corresponding restriction enzymes. The *Dictyostelium discoideum* fourth filamin domain (ddFLN4) was inserted between the ybbR tag and VBS flanked by GSGS linker to generate ybbR–ddFLN4–VBS. For protein expression, DNA constructs were transfected into *Escherichia coli* BL21(DE3)-CodonPlus cells, grown overnight at 37°C, and induced with 0.2 mM isopropyl β-d-1-thiogalactopyranoside at OD 0.8 (600 nm). After 16 h at 18°C, cells were resuspended in lysis buffer (phosphate-buffered saline (PBS), 10 mM imidazole supplemented with 10 μg/mL DNase and 100 μg/mL lysozyme), sonicated (3 × 5 min), and centrifuged down for 30 min at 40,000 g. Lysates were filtered (0.45-μm followed by 0.22-μm filter) and loaded onto a HisTrap Ni Sepharose Column (GE Healthcare) for purification via the 6xHis tag. Equilibration and washing steps (PBS with 10 mM imidazole) were followed by elution (PBS with 250 mM imidazole) into 1-mL fractions, which were analyzed by gel electrophoresis. For storage at −80°C, the proteins were dialyzed overnight at 4°C against PBS containing 5% glycerol and were shock frozen in liquid nitrogen. Chromatography-purified VBS peptides of 22 aa in length were purchased (peptides&elephants, Henningsdorf, Germany). Each peptide was flanked at both ends with a GSGS linker and contained an N- or C-terminal cysteine residue (C-GSGS-**VBS**-GSGS or GSGS-**VBS**-GSGS-C).

Attachment chemistry for AFM experiments

AFM cantilevers (Biolever Mini 40TS; Olympus, Tokyo, Japan) and glass coverslips (diameter = 24 mm) were aminosilanized and coated with NHS-PEG5000-Maleimide, as described in (32). Two different strategies for immobilization were used: Sfp-mediated reaction via the ybbR tag to NHS-PEG5000-Maleimide coated with coenzyme A and thiol-coupling of cysteines directly to maleimide groups (33). Cantilevers coated with NHS-PEG5000-Maleimide were directly immersed in 25-μL droplets of 0.5–1 mM VBS peptide containing C- or N-terminal cysteine residues. For immobilization of vinculin, glass coverslips coated with NHS-PEG5000-Maleimide were incubated for 1.5 h with 1 mM coenzyme A. Vd1 protein (50–100 μM) containing a C- or N-terminal ybbR tag was mixed with Sfp-synthase (15 μM) and incubated for 1 h at room temperature. For preparation of surfaces, either small drops of 3 μL were pipetted onto the glass slide or small drops of 60 μL were pipetted between a sandwich of two glass slides. After incubation with protein or peptide, both cantilevers and slides were rinsed with PBS. Glass slides were mounted into custom-designed AFM holders, and cantilevers were immobilized on glass cones using vacuum grease.

AFM-SMFS measurements

A custom-built AFM similar to the one described in (34) was used in the force spectroscopy mode to measure retraction curves in a fully automated way for different pulling velocities. If not noted otherwise, the standard

retraction velocity was 800 nm/s. During the measurement, the cantilever (Biolever Mini 40TS; Olympus, Tokyo, Japan) was moved by 100 nm between every approach-retraction cycle to sample different spots on the protein-coated surface. Cantilevers were calibrated after each measurement to determine their exact stiffness (35). Data were analyzed using a custom-written program for Python 2.7.

SMD/MD methods

The starting coordinates for the simulations were taken from the Protein Data Bank (PDB). The crystal structures for the Vd1 in complex with TlnVBS11 and TlnVBS58 were only solved for the proteins derived from chicken (cVinculin and cTalin) but both have very high sequence and structural identity to the human homologs (hVinculin and hTalin). cVd1 and hVd1 differ only in five positions, and most mutations are very conservative. None of them is directly involved in VBS binding, and the VBSs themselves are completely identical between the two organisms. We are thus confident that our results are not significantly influenced by this choice. We truncated terminal residues to avoid increased simulation time or system size due to unstructured regions. We used the following four structures: cVd1(1–253):cTlnVBS11(821–842) PDB: 1ZVZ (15); cVd1(1–251):cTlnVBS58(2345–2365) PDB: 1ZW2 (15); hVd1(1–253):IpaA1(611–631) PDB: 2GWW (17); hVd1(1–251):hActVBS(741–764) PDB: 1YDI (16). The missing H1-H2 loop (residues 29–35) was modeled with MODELER (36). The ad hoc model of full-length vinculin head-talin VBS11 is based on the structures of hVcl PDB: 1TR2 (37) and the Vd1-talin VBS11 PDB: 1ZVZ (15). We first deleted the tail domain and the proline-rich linker from the full-length structure. Then, we aligned the Vd1b subdomains of both structures and replaced the unbound Vd1a with the bound form. The simulations were set up with the QwikMD plug-in in VMD (38), and simulations were performed with NAMD2.12 (39). The plug-in solvated the protein in TIP3P water, charges were neutralized with NaCl, and the final NaCl concentration was set to 0.15 M. Simulations were performed using a 2-fs time-step, a pressure of 1 bar, and a temperature of 310 K, controlled with a Langevin baro- and thermostat. Simulations were run with periodic boundary conditions and particle mesh Ewald electrostatics. The system was first minimized for 2000 steps, then stepwise heated to 310 K over 145,000 steps, and subsequently equilibrated for 1 ns. During minimization, annealing, and equilibration, restraints were kept on the protein backbone atoms, with a force constant of 2 kcal/(mol $\times$ Å^2). For the SMD runs, the C-terminal residue of Vd1 was restraint with a force constant of 2 kcal/(mol $\times$ Å^2), and a moving restraint with a force constant of 7 kcal/(mol $\times$ Å^2) was put on either the N- or the C-terminus of the VBS depending on the pulling geometry. The equilibrium position of the SMD restraint was moved with 1 Å/ns (2 Å/ns for the full-length model). For the equilibrium molecular dynamics simulations, we used the same protocol for the equilibration phase. In the production runs, we restrained the lower part of Vd1b to avoid rotation of the protein in the water box, which allowed us to use a smaller box size. This is justified because we were only interested in the polar interactions between Vd1a and the VBS, which was not influenced by the restraints. Analysis was performed with in-house VMD tcl scripts and pycontact (40).

RESULTS

Performing AFM-SMFS of the first vinculin head domain in complex with VBS peptides

To measure dissociation of VBS from vinculin's first head domain under force, we employed AFM-SMFS. Short peptides for talin VBS11, talin VBS58, α-actinin VBS, and *Shigella* IpaA VBS1 were covalently attached to a cantilever tip either at their C- or N-terminus via a cysteine (α-actinin only N-terminus). The first vinculin head domain Vd1 (aa 1–258) was immobilized on the surface by covalent attachment to polymer linkers via a ybbR tag at its C-terminus (Fig. 2). We used a custom-built AFM (34) to approach the surface to induce complex formation and retracted the cantilever at a constant velocity of 800 nm/s. Cantilever retraction stretches the polymer linker, and the resulting force induces protein unfolding. As all other bonds in the system are covalent, the final rupture force peak in the AFM trace corresponds to the rupturing of the receptor-ligand complex Vd1-VBS.

Multiple pathways preceding rupture are seen for C-terminal pulling of VBS from talin and *Shigella* IpaA1

First, we probed Talin VBS11 and VBS58 as well as *Shigella* IpaA VBS1 peptides linked to the cantilever via their C-termini (Fig. 2 *A*). For this pulling geometry, our data revealed two prominent unfolding pathways for talin VBS58: a single peak followed by rupture of the complex and an unfolding pattern consisting of an intermediate peak followed by a second contour length increase of 56–58 nm, with mean rupture forces between 45 and 60 pN (Fig. 2 *A*). Dissociation of Vd1 from *Shigella* IpaA VBS1 occurred at comparable forces of 45–60 pN; however, the number of unfolding events with an intermediate step increased to half of the events. In contrast, talin VBS11 showed almost no direct unbinding at the length of the polymer linker ($\sim$50 nm) but an additional unfolding pathway with two intermediate peaks and a higher rupture force. This resulted in a bimodal distribution of rupture forces, which can be separated into a high-force (>60 pN) and low-force (<60 pN) population (Fig. 2 *A*).

N-terminal pulling of VBS from talin and *Shigella* IpaA leads to similar rupture forces but different force-extension traces

To test how the relative pulling direction affects the mechanical stability, the N-terminus of talin VBS11 and VBS58 or *Shigella* VBS IpaA1 was linked to the cantilever tip (Fig. 2 *B*). Although pulling these VBSs from their C-terminus yielded clearly distinguishable two-step unfolding, such events only rarely appeared when pulling VBSs from their N-terminus (Fig. 2 *B*). Most traces contained only a single extension. The mean rupture forces for the Vd1-VBS interaction were not significantly different from C-terminal pulling; however, the high-force populations for VBS11 disappeared. Interestingly, a new behavior was observed for the bacterial *Shigella* IpaA VBS1, consisting of a second peak at low (30–40 pN) forces (Fig. 2 *B*). In summary, we find that forces are similar for both pulling directions (Fig. 2; Table S2). However, there is a significant

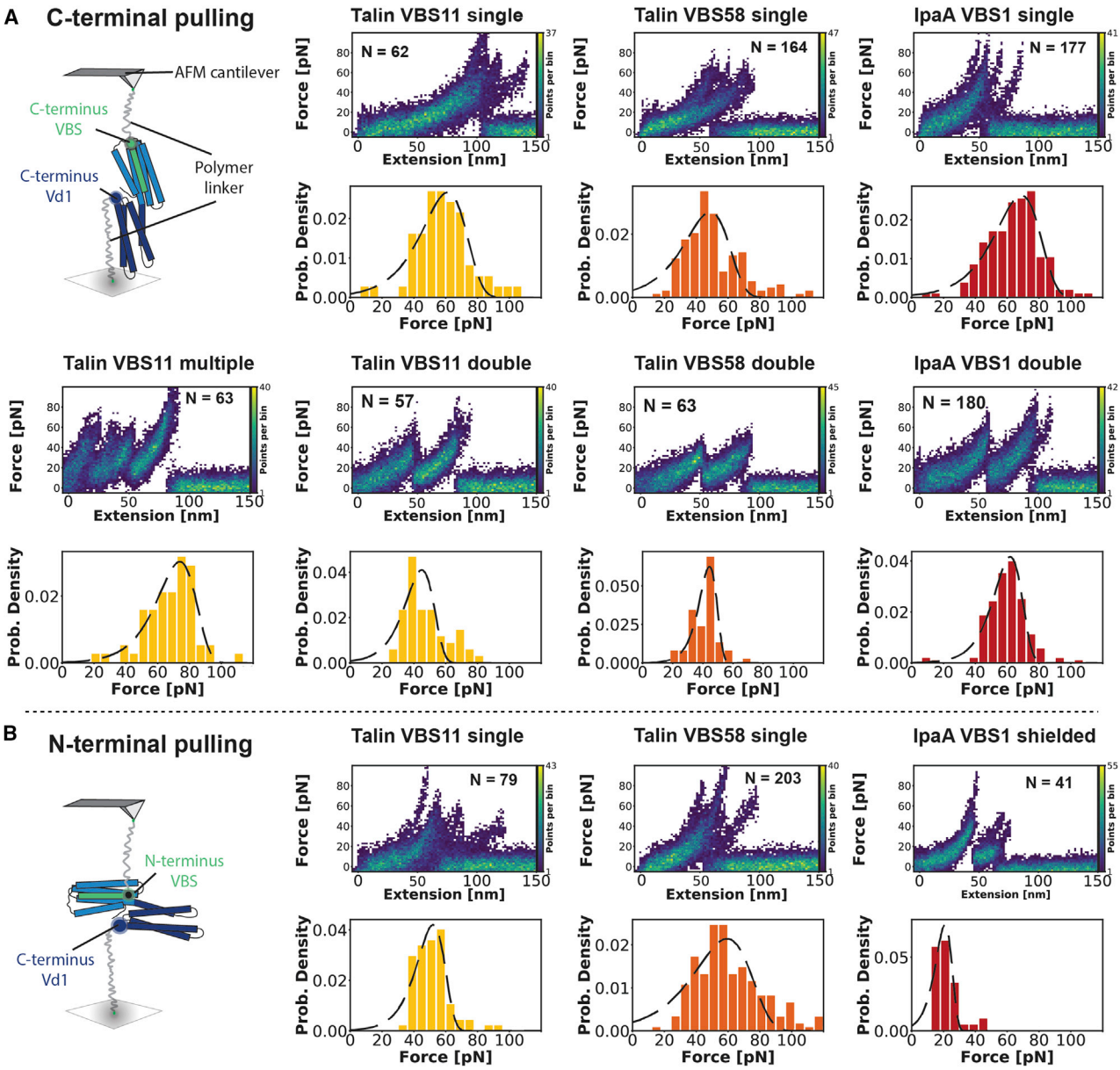

FIGURE 2 AFM-SMFS data showing directional dependence of the Vd1-VBS complex rupture. Force-extension traces from AFM-SMFS experiments using the first vinculin head domain (Vd1) C-terminally anchored to a polymer linker on the surface via a ybbR tag and different VBSs (talin VBS11, talin VBS58, IpaA VBS1), which were linked to the cantilever by a C- or N-terminal cysteine, were overlaid for representative experiments. Histogram of final rupture forces including a Bell-Evans fit is shown below (exact values are given in Table S2). (*A*) C-terminal pulling direction: for all VBSs, an extension pattern consisting of two peaks can be observed. Only talin VBS11 shows a population of high-force traces with multiple unfolding peaks. (*B*) N-terminal pulling geometry: in contrast to C-terminal pulling, no double-peak events are observed in the N-terminal pulling geometry. Only IpaA VBS1 shows unfolding of Vd1 exceeding the polymer extension length. To see this figure in color, go online.

difference in the unfolding pattern between the two geometries for all VBSs.

SMD simulations reveal atomistic details of the Vd1-VBS interaction under tension

To gain a better understanding of what causes the differences in the unfolding trajectories between pulling directions that we observed during AFM-SMFS experiments, we used SMD simulations. This allowed us to obtain a more detailed picture of the underlying conformational changes. To mimic the conditions of the experiment, we performed constant velocity SMD, using the crystal structures of the four Vd1-VBS complexes probed by AFM as starting coordinates. Again, we restrained the C-terminus of Vd1 and pulled on either terminus of the VBS. Restriction of the computationally accessible timescale requires a much higher pulling velocity (speed of 0.1 m/s, simulation time of 100 ns).

Two major classes of events can be distinguished in SMD: dissociation of VBSs from Vd1 and events in which VBSs remained bound until the end of the simulation time. In the latter case, the C-terminal vinculin subdomain Vd1b started to unfold, either from its C-terminus (helix H7 in Fig. 1 *C*) or its N-terminus (helix H4b in Fig. 1 *C*) (Fig. S1). Because of the high computational cost of the simulations, we were not able extend them until complete unfolding of the Vd1b subdomain takes place, but we expect that the subdomain becomes more and more destabilized as the unraveling proceeds. Our simulations thus capture rupture events as seen in those AFM force curves that show only a single peak with events in which the VBS peptide unbinds without Vd1 unfolding (Fig. 3, *A* and *C*; Videos S1, S2, and S3). Accordingly, those with two or more peaks are attributed to events in which Vd1b unfolds before VBS unbinding (Fig. 3, *B* and *D*; Videos S4, S5, and S6). This is in good agreement with the observed contour length increment of 56–58 nm between the first and the final peak in the AFM experiment. AFM traces with more than two maxima most likely correspond to cases in which Vd1b forms a stable unfolding intermediate that could not be detected by our simulations. A deeper analysis of the SMD results revealed that the trajectories can be further divided into those in which the Vd1a-Vd1b interface remains mostly unperturbed and those in which kinking of the helix H4 leads to a large relative reorientation of the two subdomains (Fig. 3). Once the complex is in this kinked conformation, the VBS peptide is seen to either unbind or remain bound while Vd1b starts to unravel. Results from the simulations are in good agreement with experimental observations—namely, that N-terminal pulling favors direct unbinding—whereas a substantial proportion of trajectories shows Vd1b unfolding for C-terminal pulling (Fig. 2; Fig. S1). Whereas N-terminal pulling allows the VBS turn-by-turn to be peeled off in a zipper-like fashion (Video S3), C-terminal pulling requires the movement of residues along the binding groove in a more shear-like fashion (Video S1).

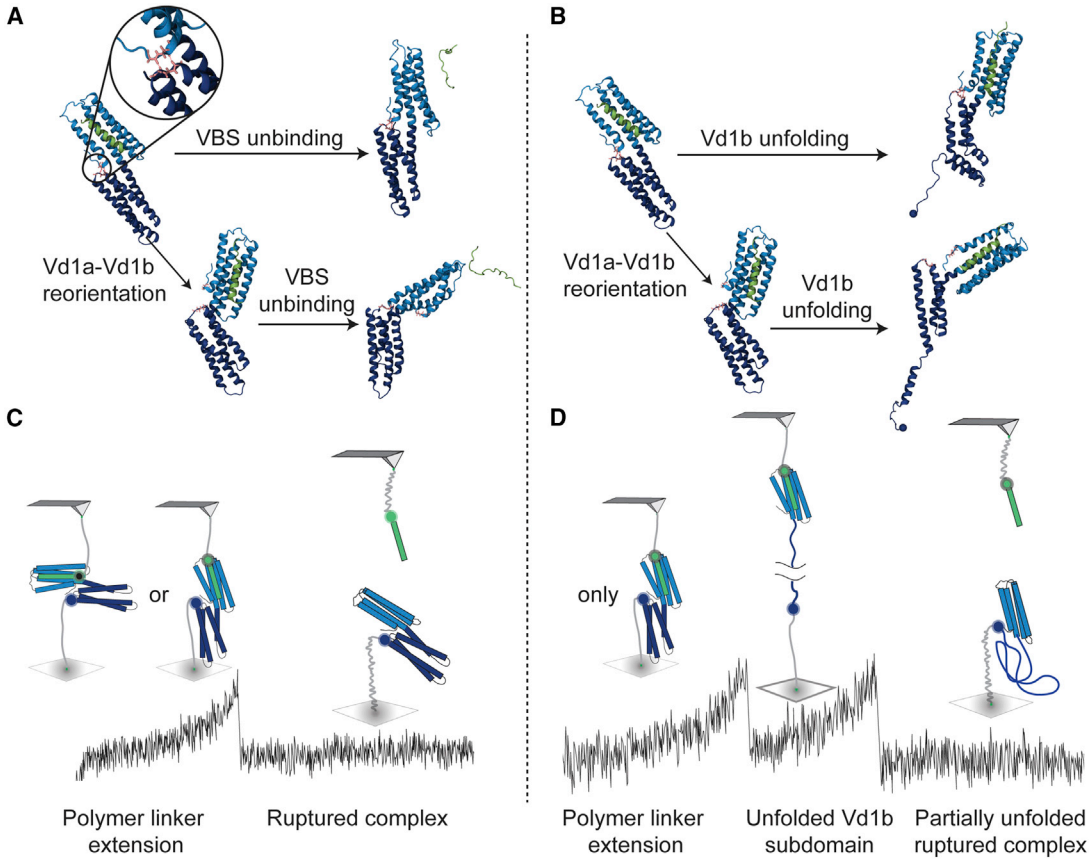

FIGURE 3 Direct unbinding of the vinculin binding peptide (*green*) from the vinculin head domain or prior unfolding of its Vd1b subdomain (shades of *blue*). (*A*) Direct unbinding of the Vd1-VBS complex is observed in experiments and simulations for both pulling directions. SMD simulations suggest that unbinding can occur before or after reorientation of Vd1 subdomains. (*B*) SMD simulations observe more events for unfolding of the Vd1b subdomain for shear-like pulling. During SMFS experiments, the prominent double-peak unfolding with a contour length increment of 56–58 nm is only observed for the shear-like pulling geometry (C-terminal for talin VBS and IpaA VBS1, N-terminal for the inverted VBS present in α-actinin). To see this figure in color, go online.

The mechanical stability of the Vd1-VBS complex is independent of helix backbone orientation

Next, we wanted to understand whether the mechanical anisotropy depends on orientation of the helix backbone. To this end, we generated a construct using the VBS of α-actinin for which the position of N- and C-terminus in the crystal structure is inverted. During AFM measurements, we observed the typical two-step unfolding for N-terminal shear-like pulling, which all other VBSs showed upon C-terminal shear-like pulling. SMD simulations revealed a higher stability for the N-terminal pulling of α-actinin with no unbinding events. In contrast, the C-terminal zipper-like pulling configuration of α-actinin VBSs showed unbinding in 8 out of 10 simulations. This demonstrates, that α-sctinin VBSs indeed act like an inverted talin VBS (Figs. S1, D and H and S2). Thus, the mechanical anisotropy between zipper-like and shear-like geometries can exist independently of helix backbone orientation.

Structural details explain directional anisotropy for Vd1-VBS unbinding

SMD revealed that VBS unbinding occurs via structurally distinct trajectories: for shear-like pulling, the VBS helix starts to unwind successively from the end where the force is applied. When the Vd1-VBS complex is disrupted, this proceeds until the VBS is either completely unfolded and unbinds, or it unbinds while it is still partially helical (Fig. 4 *A*; Video S1). In some trajectories of talin VBS58, dissociation was preceded by a stepwise sliding of the VBS helix within its binding groove, which led to displacements of the nonpulling terminus of up to 15 Å (Fig. 4 *B*; Video S2). Yet depending on the type of VBS, a significant subset of simulations did not lead to a complete unbinding, but instead, the unfurling of the VBS helix was stalled, or even reverted, after a few residues, and Vd1b started to unravel (Fig. 4 *E*; Video S5). In 9 of 10 simulations for VBS11 and 5 of 10 simulations for VBS58, the helix-to-coil transition of the VBS was arrested by the formation of a short

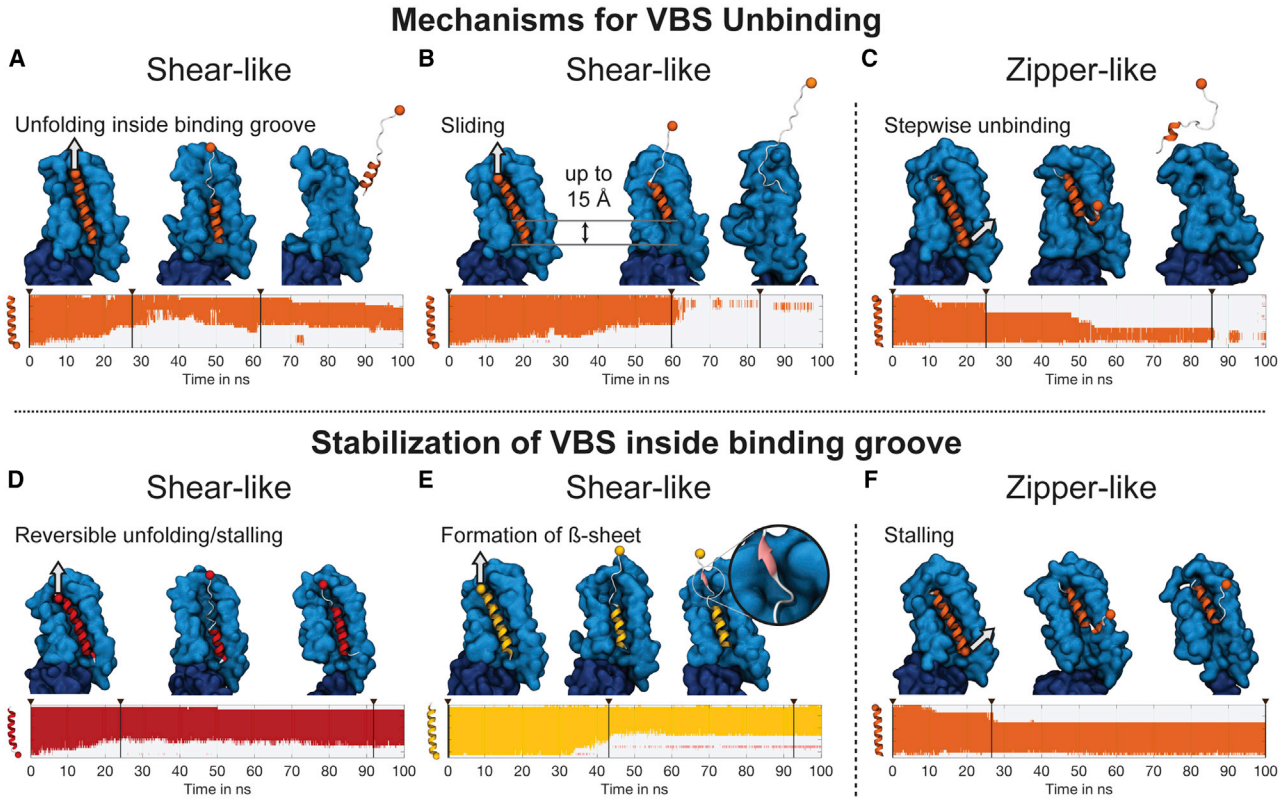

FIGURE 4 Atomistic details that increase the mechanical stability of the Vd1 (*blue*)-VBS for shear-like pulling out of the helix from the binding groove. Representative snapshots from SMD trajectories illustrating different responses of the Vd1-VBS (full data sets: Fig. S4). Kymographs show the time evolution of the secondary structure of the VBS peptide (top: N-terminus, bottom: C-terminus). Solid colors (*red*, *yellow*, *orange*) represent α-helical structure, unstructured regions are depicted in gray, and pink is used for β-sheet structures. Black arrows indicate representative frames, which are shown in the upper part of the panel. Shear-like pulling of Vd1-VBS complex can lead to direct unbinding via two mechanisms: (*A*) partial or complete unfurling of VBS helix inside the binding groove and (*B*) stepwise sliding of the whole VBS peptide before unbinding. This leads to a shift of the complete VBS of up to 15 Å. (*C*) Zipper-like pulling of Vd1-VBS can lead to direct unbinding; however, in contrast to the shear-like pulling, a turn-by-turn helix unbinding is observed. For shear-like pulling, the following mechanisms impede unbinding: (*D*) stalling of VBS unfolding, in some cases combined with refolding of the helix; (*E*) formation of a β-sheet between a loop in Vd1 and partially unfurled VBS; and (*F*) in zipper-like direction, the VBS unfolding can also get stalled at specific amino acids (Fig. S6). To see this figure in color, go online.

β-sheet between the H1/H2 loop and unfolded VBS residues (Fig. 4 *D*; Video S4). In the zipper-like geometry, a stepwise unfolding of whole helical turns was observed before the VBS would eventually unbind (Fig. 4 *C*; Video S3). VBS unfolding was preferentially stalled at certain amino acids (Fig. 4 *F*; Fig. S3); however, the additional mechanisms to prevent unbinding, like formation of a β-sheet, were not observed (Video S6). To investigate more closely how the unfolding pathways depend on the amino acid sequence of individual VBSs, we performed further in silico mutation studies on talin VBS11. A detailed analysis for all simulations can be found in the Supporting Material. In summary, the unbinding mechanism of the complexes is governed by a sophisticated interplay between bulky amino acids and H-bonds (Fig. S3–S5).

Semiquantitative comparison of mechanical stability of Vd1-VBS complexes

Surprisingly, our AFM data showed that the rupture forces needed to dissociate the Vd1-VBS complex did not differ greatly between zipper-like and shear-like geometry. However, we did observe differences in the ratio of direct unbinding versus unbinding after vinculin Vd1 unfolding, both between different VBS sequences and, even more pronounced, between pulling geometries. The zipper geometry generally favored direct unbinding, whereas both processes occurred in the shear geometry (Figs. 2 and 3). This competition between the pathways suggests that their force distributions are overlapping in our pulling velocities, which biases the measured forces, as described in (41). As a result, we observe more direct unbinding events the smaller the mean rupture force is, compared to the unfolding force of Vd1b and vice versa (Fig. S3). The ratio of unfolding to direct unbinding (UF/UB) derived from AFM experiments can thus be used to compare the mechanical stability of the complexes semiquantitatively. For shear-like pulling, both AFM experiments and simulations suggest that talin VBS58 (UF/UB $\approx$ 0.4) forms the least stable complex and that talin VBS11 (UF/UB $\approx$ 2) forms the most stable complex. The stability of IpaA VBS1 (UF/UB $\approx$ 1) is in an intermediate regime. In the zipper-like pulling geometry, the two tested talin VBSs unbind easily (UF/UB $\approx$ 0), whereas IpaA VBS1 binds stably, and Vd1 always unfolds before unbinding. Because we observed no relationship between the mechanical stability and the equilibrium affinity of the VBS for Vd1 (Fig. 2; Fig. S7), the distribution of vinculin within adhesions can be fine-tuned by an intricate combination of the mechanical stability of VBS-containing domains, the affinities of the exposed VBSs for vinculin, and the loading geometries of the Vd1-VBS linkages. The simple UF/UB criterion suggests that talin VBSs bind more stably in the shear-like compared with the zipper-like geometry. However, a direct comparison between pulling geometries is only possible when Vd1b unfolds at the same forces in both configurations. From Fig. 2, it becomes apparent that this is not necessarily the case because force is applied once antiparallelly (shear) and once perpendicularly (zipper) to the long axis of the helix bundle.

The anisotropic force response is recapitulated using full-length vinculin head

Because this issue is difficult to address experimentally and because force transmission through the C-terminus of Vd1 is artificially introduced through the design of our truncated model system, we extended our in silico approach to the much bigger complex in which a VBS helix is bound to the full-length vinculin head. This setup leads to a very similar force geometry but a different force transduction pathway (Fig. 5). By combining the crystal structures of vinculin and the Vd1-TalinVBS11 complex, we created an ad

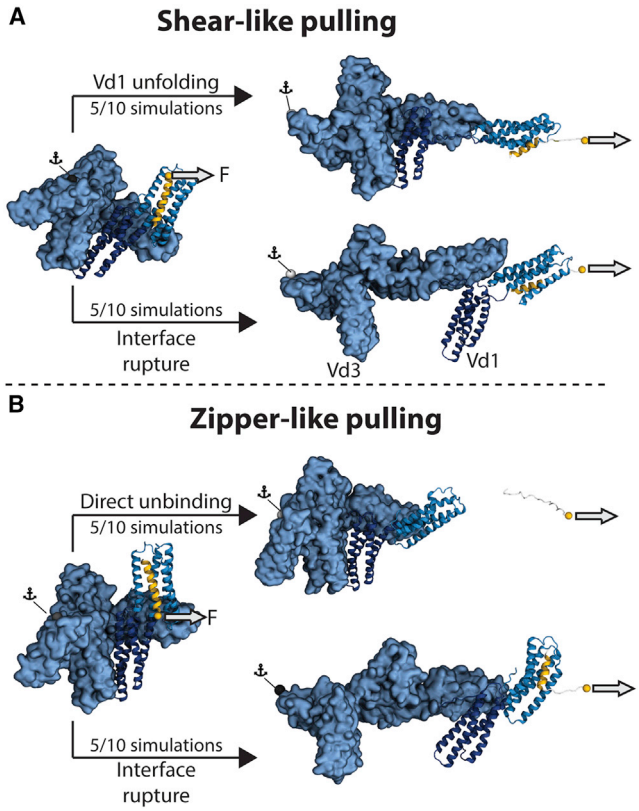

FIGURE 5 Simulation of full-length vinculin head for shear- and zipper-like pulling of talin VBS11. (*A*) When Talin VBS11 is pulled out of the vinculin binding groove by applying force to its C-terminus in a shear-like configuration, major conformational changes of vinculin can be observed: extension of the vinculin head domains, which leads to a kinking of the Vd1a-Vd1b interface, the rupture of the Vd1-Vd3 interface, and partial unfolding of helices in the vinculin head. (*B*) In the zipper-like geometry, when pulling on its N-terminus, talin VBS11 can unbind from the vinculin head without prior extension. When the talin helix remains bound, it induces extension of the vinculin head by rearrangements of vinculin subdomains. To see this figure in color, go online.

hoc model of the vinculin head-TalinVBS11 complex (see Materials and Methods). VBS11 was chosen as a binding partner for closer investigation because it shows the biggest difference in its geometry-dependent force response, both in the experiments and in the simulations. Indeed, we were able to reproduce a differential stability for the two geometries. In accordance with our semiquantitative model, we again observed more direct unbinding for the zipper-like geometry (5/10 simulations) than for shear-like pulling (0/10 simulations) (Fig. 5; Videos S7 and S10). Moreover, the kinking between Vd1a and Vd1b as a response to force occurred again in some cases.

The full-length vinculin head responds to VBS helix pulling by rupture of the Vd1-Vd3 interface and major rearrangement of its subdomains

The simulation of the full-length vinculin head led us to another striking observation. Besides Vd1 unfolding, we frequently saw the rupture of the Vd1-Vd3 interface, leading to a large, force-induced reorganization and extension of vinculin head of up to 8 nm (Fig. 5; Videos S8 and S9). This conformational change is solely driven by rearrangement of the head domains and requires no unfolding thereof. For both shear- and zipper-like pulling, vinculin extended in half of the cases (5/10 simulations). In contrast, further simulations suggest that the Vd1-Vd3 interface remains intact when force is applied parallel to the VBS (Fig. S8), adding an additional layer of directional sensitivity to the force response of the Vh-VBS complex. Vd1 and Vd3 are connected by a hinge-like interface that zips open relatively easily for both force geometries shown in Fig. 5. In contrast, when the force is applied parallel to the VBS, the Vd1-Vd3 interface is loaded in a shear geometry, and the two domains remain connected (Fig. S8).

DISCUSSION

Understanding the molecular force response of vinculin with atomistic-level structural detail is an essential milestone on the way to a full description of force transmission through adhesion sites because it serves as a central connector that interacts with numerous competing binding partners and assumes multiple roles in different adhesion types (1,2). After the discovery by Huang et al. that vinculin's tail domain forms a directionally asymmetric catch bond with F-actin (42), we were able to expand the picture by showing that the vinculin-head-VBS interaction also exhibits anisotropic mechanical stability. We found that force application in a zipper-like (N-terminal) pulling geometry is associated with increased dissociation of the VBS, whereas the complex is more stable in the shear-like (C-terminal) pulling geometry (Figs. 2 and 5). Furthermore, our data suggest that intramolecular interfaces within vinculin head are also sensitive to force direction and that their rupture can trigger large conformational changes (Fig. 5). This furthers the notion that vinculin is not only a passive force transduction unit but can rather sense force direction and modulate the interaction with its binding partners accordingly.

Simulations performed by Huang et al. suggest that the anisotropy in the mechanical stability of the vinculin-actin connection strongly biases the polarity distribution of actin filaments undergoing retrograde flow (42). Based on our findings, we further propose that vinculin can not only detect and modulate filament polarity with its tail domain but also sense relative filament orientation with its head domain. This could be especially relevant in nascent adhesions, emerging at the leading edge of the cell in the lamellipodium. Because actin fibers in this region are highly unaligned (43), vinculin and, e.g., talin can interact with filaments pointing in different directions (Fig. 6 *A*). Our data suggest that such a configuration results in zipper-like pulling, leading to faster dissociation of the complex (Fig. 6 *A*). In mature adhesions, most vinculin is presumably pulled along the direction of talin, leading to a loading of the VBS in a shear geometry, albeit in the opposite direction than in our experiments (Fig. 6 *C*; (8)). However, it is likely that the complex is also stable in this direction, allowing vinculin to reinforce the link between talin and F-actin efficiently (Fig. 6 *C*). Indeed, a recent study shows that the tension across talin correlates with the alignment of actin filaments: high tension is only observed in regions of parallel F-actin bundles, whereas areas of reduced tension across talin show a decrease in filament alignment (44).

The high spatiotemporal resolution of atomistic SMD simulations gave us insights into the structural mechanisms that govern the differences in stability. Whereas the domains of transmembrane adhesion receptor families like cadherins or integrins are dominated by β-sheet folds, the intracellular adhesion protein families examined in this study are mostly α-helical. In β-sheet proteins, the number of backbone hydrogen bonds that need to be broken simultaneously regulates the differences in unfolding strength of shear versus zipper geometry. In this case, a clear force hierarchy with high forces for shear and low forces for zipper arrangement has been reported (45,46). In contrast, unbinding of the α-helical vinculin-VBS complex is mediated by side chain interactions stabilizing the helix bundles. In the shear-like geometry, residues experience high friction as they get pulled along and eventually out of the groove (Fig. 4, *A*, *B*, *D*, and *E*). We found that mechanical strength in this geometry is modulated by complex synergies of hydrophobic and polar contacts, which vary between VBSs. A recent study has shown that these interactions stabilize the helical conformation of the VBS so strongly that vinculin binding can trigger a coil-to-helix transition in mechanically overstretched talin (47). Interestingly, we can partially observe this process in our simulations when we see refolding of the VBS in the binding groove under load (Fig. 4 *D*). In contrast, in the zipper-like configuration, the force acts

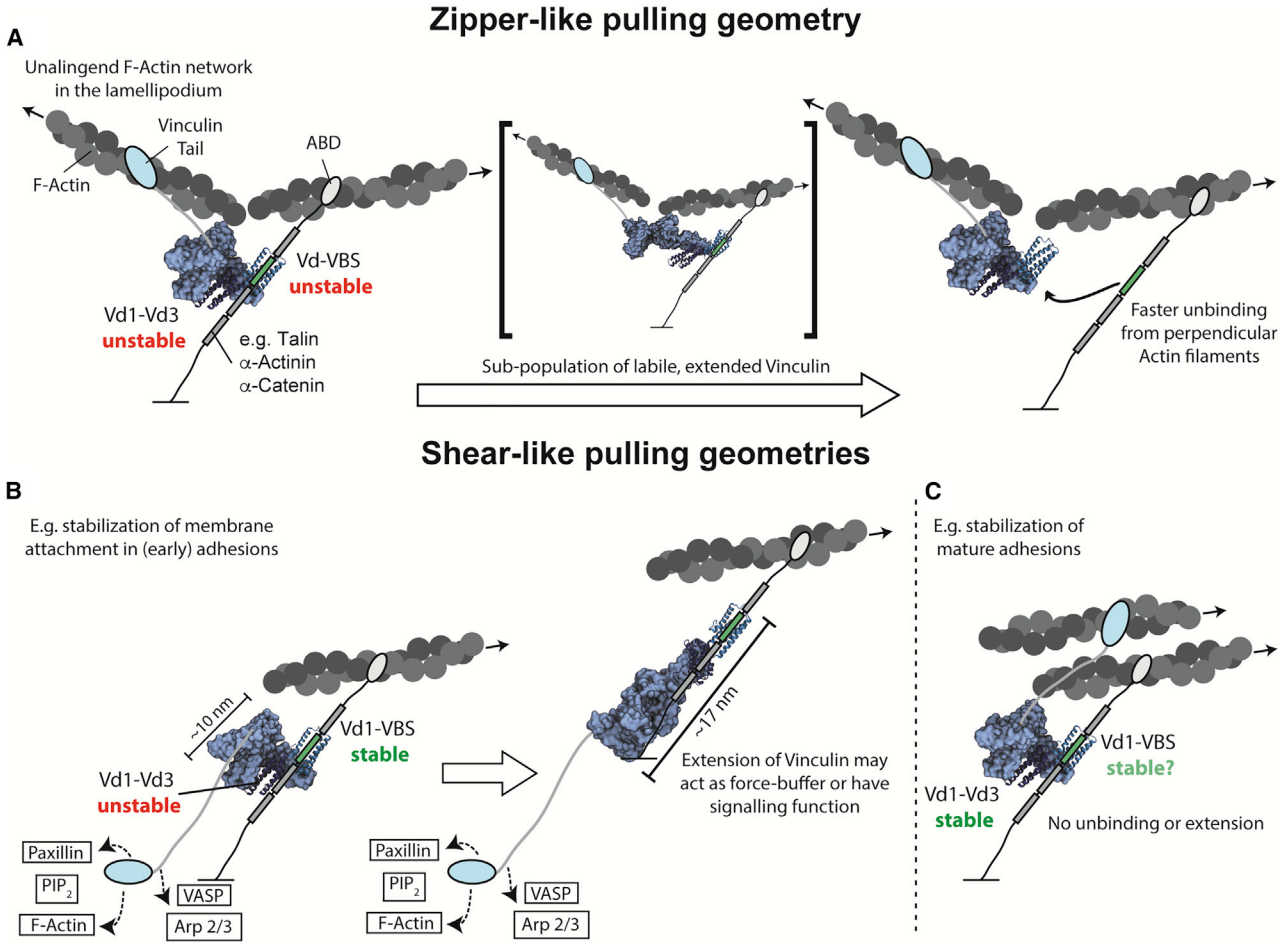

FIGURE 6 Possible force responses of the vinculin-VBS complex to different pulling geometries in the cell. (*A*) Zipper-like pulling of the vinculin-VBS complex arises when actin fibers are not aligned (e.g., in the lamellipodium). This results in a configuration in which both the Vd1-VBS and the Vd1-Vd3 interfaces are destabilized. This should ultimately lead to increased dissociation of vinculin from the VBS, with a subpopulation of the vinculin molecules extending before unbinding. (*B*) Vinculin tail can bind to PIP_2, paxillin, or F-actin. The linker region can also interact with other proteins, like VASP or Arp2/3. This can result in shear-like pulling, which stabilizes the vinculin-VBS interface and promotes extension of vinculin head upon force application. (*C*) Engagement to parallel actin fibers results again in a shear-like loading of the Vd1-VBS interface that is presumably stable under force; the same is true for the Vd1-Vd3 interface. In such a configuration that might be prevalent in mature adhesions, neither unbinding nor vinculin head extension is favored. To see this figure in color, go online.

perpendicular to the binding groove, and the residues experience less drag as they get pulled out one by one. In this geometry, unbinding is regulated mostly by the extraction of conserved bulky hydrophobic side chains (Fig. 4, *C* and *F*; Table S1). These different unbinding mechanisms explain why we see a larger sequence dependence for shear-like pulling. These differences might reflect an adaptation to the distinct mechanical challenges that each VBS experiences. For example, talin VBS11, which formed the most stable complex, is exposed early in adhesion formation, possibly even before talin extension (48,49). It is thus tempting to speculate that the exceptional stability of talin VBS11 is a mechanism to stabilize talin's membrane attachment in very early adhesions (Fig. 6 *C*; (23)). Intriguingly, deletion of vinculin leads to a reduced number of nascent adhesions in the lamellipodium (50). On the other hand, a recent study that challenges the physiological vinculin binding activity of talin VBS58 could explain its low mechanical stability (26). If this VBS is not engaged to vinculin in vivo, there is no need to evolve high mechanical stability.

Although the measured rupture forces of 45–60 pN exceed the tension that adhesion molecules experience under physiological conditions, it is important to note that forces derived from AFM-SMFS measurements and SMD simulations cannot be directly related to forces under physiological conditions because of the higher pulling speed (AFM = 800 nm/s, SMD = 0.1 m/s, in vivo = 50–100 nm/s (51)). Extrapolation of rupture forces with the Bell-Evans model (52) to lower loading rates for the IpaA VBS1-Vd1 complex suggests that under physiological conditions, unbinding occurs already between 20 and 30 pN (Fig. S9). Even though these forces are still higher than

those reported from genetically encoded tension sensors (19,20), the extrapolation brings the experimentally determined VBS unbinding and unfolding forces in the same force range as reported for the more stable talin bundles (53). Further unraveling of talin could thus act as a force buffer that competes with vinculin unbinding. So far, no absolute upper maximum of forces occurring across vinculin has been determined by means of tension sensor measurements. These measurements average over a large ensemble of molecules that are present at adhesion sites. However, a subset of vinculin might still experience higher force, especially in tissues that have to withstand high external mechanical load. The challenges associated with deriving force distributions from tension sensors has been recently reviewed in (54). Furthermore, the commonly used tension sensors might not be optimally designed to assess forces transmitted through the vinculin head. The fluorophores are inserted between the binding sites for actin-binding proteins (e.g., VASP, Arp2/3) that interact with the proline-rich linker and the tail domain (19). Therefore, they only allow measurement of the tension between these two points, which is not necessarily equivalent to the tension transmitted through the vinculin-VBS interface. This is demonstrated by the fact that the sensors still register load on vinculin, even when its VBS binding ability is abolished (55).

Our simulations of the full-length vinculin head in complex with talin VBS showed that force across vinculin can lead to large conformational changes triggered by the dissociation of the interface between the first (Vd1) and the third (Vd3) head domain. The probability of this interface rupture is again direction dependent (Fig. 6). Interestingly the equivalent interface in the homologous protein α-catenin has been previously reported to be flexible and mechanically labile (56,57). When the crystal structure of human vinculin was first solved, the authors hypothesized that the release of the tail domain could destabilize the compact conformation of the head domain even in the absence of force (57). Our data suggest that, once vinculin is under tension, the equilibrium shifts even further toward a more open, elongated state. The recently published structure of full-length talin suggests an analogous mechanism for the transition from its compact, autoinhibited conformation to its fully extended form (48). We want to bring forward two hypotheses for the biological function of vinculin head extension. First, it might be a mechanism to protect the bond to the VBS from large force fluctuations, preventing undesired mechanical failure of the cell anchorage, as previously shown for the uncoiling of fimbriae extending the lifetime of the FimH-Mannose catch bond (58). Second, vinculin, like other force-bearing adhesion proteins, might act as a direction-dependent mechanochemical signaling switch (59). This implies that tension either opens cryptic binding sites or prevents interactions with certain binding partners. An example for the latter would be the intramolecular interaction with its tail domain. In the closed conformation, the tail domain binds to almost all domains of the head simultaneously, which is not possible in the extended conformation of the head. Vinculin head extension should destroy this multivalent binding motif and thus reduce the head-tail affinity. On the other hand, mechanoenhanced binding of MAPK1 to the vinculin head has been recently reported (60,61). However, we want to point out that our observations are derived from an ad hoc model of the Vh-VBS complex. The results should thus not be treated as precise structural models but should rather motivate to explore the structural plasticity of the vinculin head experimentally in the future.

CONCLUSIONS

Our combined AFM and SMD simulation studies provide fundamentally new insights into the mechanical design of vinculin in complex with its binding partners. We suggest new mechanisms for how vinculin can act as a mechanosensitive logical gate that converts the inputs force, geometry, and magnitude into distinct structural outputs with potentially different biological function. We have depicted three possible outcomes for a simple system consisting of vinculin, a VBS-bearing protein, and F-actin in Fig. 6. The outputs are not to be understood as deterministic but rather probabilistic and will most likely further depend on the exact angle between the VBS and the pulling direction. The force response gets even more complicated if the directionally asymmetric catch bond between vinculin tail and F-actin is taken into account (42). Even though our reduced model system does not do justice to the vast complexity that arises in actual adhesion sites, our work offers a new perspective on force transduction through vinculin that will inspire further studies in the future.

SUPPORTING MATERIAL

Supporting Material can be found online at https://doi.org/10.1016/j.bpj.2019.12.042.

AUTHOR CONTRIBUTIONS

C.K., L.B., and D.A.P. designed the experiments with input from H.E.G. and V.V. C.K., S.M.S., K.M., and D.A.P. performed experimental work. L.B. performed all SMD simulations and analysis. L.F.M. and M.S.B. wrote software and contributed to AFM data analysis. C.K., L.B., and V.V. wrote the manuscript with input from all authors.

ACKNOWLEDGMENTS

The authors thank Leonard Schendel and Aron Venczel for fruitful discussion and general support. We are thankful for the help of Thomas Nicolaus and Angelika Kardinal with preparation of surfaces for AFM and protein expression.

This work was funded by the Deutsche Forschungsgemeinschaft (DFG, German Research Foundation) – Project-ID 201269156 – SFB 1032, by

ETH Zurich, and by a grant from the Swiss National Supercomputing Centre (CSCS) under project ID s791 and s891. C.K. was supported by the Fritz Thyssen Foundation.

REFERENCES

1. Goldmann, W. H. 2016. Role of vinculin in cellular mechanotransduction. *Cell Biol. Int.* 40:241–256.
2. Carisey, A., and C. Ballestrem. 2011. Vinculin, an adapter protein in control of cell adhesion signalling. *Eur. J. Cell Biol.* 90:157–163.
3. Geiger, B. 1979. A 130K protein from chicken gizzard: its localization at the termini of microfilament bundles in cultured chicken cells. *Cell.* 18:193–205.
4. Sydor, A. M., A. L. Su, …, D. G. Jay. 1996. Talin and vinculin play distinct roles in filopodial motility in the neuronal growth cone. *J. Cell Biol.* 134:1197–1207.
5. Nolz, J. C., R. B. Medeiros, …, D. D. Billadeau. 2007. WAVE2 regulates high-affinity integrin binding by recruiting vinculin and talin to the immunological synapse. *Mol. Cell. Biol.* 27:5986–6000.
6. Weiss, E. E., M. Kroemker, …, M. Rüdiger. 1998. Vinculin is part of the cadherin-catenin junctional complex: complex formation between alpha-catenin and vinculin. *J. Cell Biol.* 141:755–764.
7. Bertocchi, C., Y. Wang, …, P. Kanchanawong. 2017. Nanoscale architecture of cadherin-based cell adhesions. *Nat. Cell Biol.* 19:28–37.
8. Case, L. B., M. A. Baird, …, C. M. Waterman. 2015. Molecular mechanism of vinculin activation and nanoscale spatial organization in focal adhesions. *Nat. Cell Biol.* 17:880–892.
9. del Rio, A., R. Perez-Jimenez, …, M. P. Sheetz. 2009. Stretching single talin rod molecules activates vinculin binding. *Science.* 323:638–641.
10. Yao, M., B. T. Goult, …, J. Yan. 2014. Mechanical activation of vinculin binding to talin locks talin in an unfolded conformation. *Sci. Rep.* 4:4610.
11. Le, S., X. Hu, …, J. Yan. 2017. Mechanotransmission and mechanosensing of human alpha-actinin 1. *Cell Rep.* 21:2714–2723.
12. Yao, M., W. Qiu, …, J. Yan. 2014. Force-dependent conformational switch of α-catenin controls vinculin binding. *Nat. Commun.* 5:4525.
13. Hytönen, V. P., and V. Vogel. 2008. How force might activate talin's vinculin binding sites: SMD reveals a structural mechanism. *PLoS Comput. Biol.* 4:e24.
14. Izard, T., G. Evans, …, P. R. J. Bois. 2004. Vinculin activation by talin through helical bundle conversion. *Nature.* 427:171–175.
15. Gingras, A. R., W. H. Ziegler, …, J. Emsley. 2005. Mapping and consensus sequence identification for multiple vinculin binding sites within the talin rod. *J. Biol. Chem.* 280:37217–37224.
16. Bois, P. R. J., R. A. Borgon, …, T. Izard. 2005. Structural dynamics of alpha-actinin-vinculin interactions. *Mol. Cell. Biol.* 25:6112–6122.
17. Izard, T., G. Tran Van Nhieu, and P. R. J. Bois. 2006. Shigella applies molecular mimicry to subvert vinculin and invade host cells. *J. Cell Biol.* 175:465–475.
18. Rahikainen, R., M. von Essen, …, V. P. Hytönen. 2017. Mechanical stability of talin rod controls cell migration and substrate sensing. *Sci. Rep.* 7:3571.
19. Grashoff, C., B. D. Hoffman, …, M. A. Schwartz. 2010. Measuring mechanical tension across vinculin reveals regulation of focal adhesion dynamics. *Nature.* 466:263–266.
20. LaCroix, A. S., A. D. Lynch, …, B. D. Hoffman. 2018. Tunable molecular tension sensors reveal extension-based control of vinculin loading. *eLife.* 7:531.
21. Austen, K., P. Ringer, …, C. Grashoff. 2015. Extracellular rigidity sensing by talin isoform-specific mechanical linkages. *Nat. Cell Biol.* 17:1597–1606.
22. Ye, N., D. Verma, …, S. Z. Hua. 2014. Direct observation of α-actinin tension and recruitment at focal adhesions during contact growth. *Exp. Cell Res.* 327:57–67.
23. Calderwood, D. A., I. D. Campbell, and D. R. Critchley. 2013. Talins and kindlins: partners in integrin-mediated adhesion. *Nat. Rev. Mol. Cell Biol.* 14:503–517.
24. Rangarajan, E. S., and T. Izard. 2013. Dimer asymmetry defines α-catenin interactions. *Nat. Struct. Mol. Biol.* 20:188–193.
25. McCann, R. O., and S. W. Craig. 1997. The I/LWEQ module: a conserved sequence that signifies F-actin binding in functionally diverse proteins from yeast to mammals. *Proc. Natl. Acad. Sci. USA.* 94:5679–5684.
26. Rahikainen, R., T. Öhman, …, V. P. Hytönen. 2019. Talin-mediated force transmission and talin rod domain unfolding independently regulate adhesion signaling. *J. Cell Sci.* 132:jcs226514.
27. Goult, B. T., T. Zacharchenko, …, I. L. Barsukov. 2013. RIAM and vinculin binding to talin are mutually exclusive and regulate adhesion assembly and turnover. *J. Biol. Chem.* 288:8238–8249.
28. Yao, M., B. T. Goult, …, J. Yan. 2016. The mechanical response of talin. *Nat. Commun.* 7:11966.
29. Kanchanawong, P., G. Shtengel, …, C. M. Waterman. 2010. Nanoscale architecture of integrin-based cell adhesions. *Nature.* 468:580–584.
30. Liu, J., Y. Wang, …, P. Kanchanawong. 2015. Talin determines the nanoscale architecture of focal adhesions. *Proc. Natl. Acad. Sci. USA.* 112:E4864–E4873.
31. Valencia-Gallardo, C., C. Bou-Nader, …, G. Tran Van Nhieu. 2019. Shigella IpaA binding to talin stimulates filopodial capture and cell adhesion. *Cell Rep.* 26:921–932.e6.
32. Zimmermann, J. L., T. Nicolaus, …, K. Blank. 2010. Thiol-based, site-specific and covalent immobilization of biomolecules for single-molecule experiments. *Nat. Protoc.* 5:975–985.
33. Ott, W., M. A. Jobst, …, M. A. Nash. 2017. Single-molecule force spectroscopy on polyproteins and receptor-ligand complexes: the current toolbox. *J. Struct. Biol.* 197:3–12.
34. Gumpp, H., S. W. Stahl, …, H. E. Gaub. 2009. Ultrastable combined atomic force and total internal fluorescence microscope. *Rev. Sci. Instrum.* 80:063704.
35. Hutter, J. L., and J. Bechhoefer. 1998. Calibration of atomic-force microscope tips. *Rev. Sci. Instrum.* 64:1868–1873.
36. Webb, B., and A. Sali. 2014. Comparative Protein Structure Modeling Using MODELLER. John Wiley & Sons, Inc., Hoboken, NJ.
37. Borgon, R. A., C. Vonrhein, …, T. Izard. 2004. Crystal structure of human vinculin. *Structure.* 12:1189–1197.
38. Humphrey, W., A. Dalke, and K. Schulten. 1996. VMD: visual molecular dynamics. *J. Mol. Graph.* 14:33–38, 27–28..
39. Phillips, J. C., R. Braun, …, K. Schulten. 2005. Scalable molecular dynamics with NAMD. *J. Comput. Chem.* 26:1781–1802.
40. Scheurer, M., P. Rodenkirch, …, T. Rudack. 2018. PyContact: rapid, customizable, and visual analysis of noncovalent interactions in MD simulations. *Biophys. J.* 114:577–583.
41. Schoeler, C., T. Verdorfer, …, M. A. Nash. 2016. Biasing effects of receptor-ligand complexes on protein-unfolding statistics. *Phys. Rev. E.* 94:042412.
42. Huang, D. L., N. A. Bax, …, A. R. Dunn. 2017. Vinculin forms a directionally asymmetric catch bond with F-actin. *Science.* 357:703–706.
43. Weichsel, J., E. Urban, …, U. S. Schwarz. 2012. Reconstructing the orientation distribution of actin filaments in the lamellipodium of migrating keratocytes from electron microscopy tomography data. *Cytometry A.* 81:496–507.
44. Kumar, A., K. L. Anderson, …, M. A. Schwartz. 2018. Local tension on talin in focal adhesions correlates with F-actin alignment at the Nanometer Scale. *Biophys. J.* 115:1569–1579.
45. Brockwell, D. J., E. Paci, …, S. E. Radford. 2003. Pulling geometry defines the mechanical resistance of a β-sheet protein. *Nat. Struct. Biol.* 10:731–737.
46. Sedlak, S. M., L. C. Schendel, …, R. C. Bernardi. 2019. Direction matters: monovalent streptavidin/biotin complex under load. *Nano Lett.* 19:3415–3421.

47. Tapia-Rojo, R., A. Alonso-Caballero, and J. M. Fernandez. 2019. Direct observation of a coil-to-helix contraction triggered by vinculin binding to talin. *bioRxiv* https://doi.org/10.1101/741884.

48. Dedden, D., S. Schumacher, …, N. Mizuno. 2019. The architecture of Talin1 reveals an autoinhibition mechanism. *Cell.* 179:120–131.e13.

49. Atherton, P., F. Lausecker, …, C. Ballestrem. 2019. Relief of talin autoinhibition triggers a force-independent association with vinculin. *J. Cell Biol.* 219.

50. Thievessen, I., P. M. Thompson, …, C. M. Waterman. 2013. Vinculin-actin interaction couples actin retrograde flow to focal adhesions, but is dispensable for focal adhesion growth. *J. Cell Biol.* 202:163–177.

51. Forscher, P., and S. J. Smith. 1988. Actions of cytochalasins on the organization of actin filaments and microtubules in a neuronal growth cone. *J. Cell Biol.* 107:1505–1516.

52. Evans, E. 2003. Probing the relation between force—lifetime—and chemistry in single molecular bonds. *Annu. Rev. Biophys. Biomol. Struct.* 30:105–128.

53. Haining, A. W. M., M. von Essen, …, A. Del Río Hernández. 2016. All subdomains of the talin rod are mechanically vulnerable and may contribute to cellular mechanosensing. *ACS Nano.* 10:6648–6658.

54. Yasunaga, A., Y. Murad, and I. T. S. Li. 2019. Quantifying molecular tension-classifications, interpretations and limitations of force sensors. *Phys. Biol.* 17:011001.

55. Rothenberg, K. E., D. W. Scott, …, B. D. Hoffman. 2018. Vinculin force-sensitive dynamics at focal adhesions enable effective directed cell migration. *Biophys. J.* 114:1680–1694.

56. Li, J., J. Newhall, …, E. Tajkhorshid. 2015. Structural determinants of the mechanical stability of α-catenin. *J. Biol. Chem.* 290:18890–18903.

57. Bush, M., B. M. Alhanshali, …, Z. Bu. 2019. An ensemble of flexible conformations underlies mechanotransduction by the cadherin-catenin adhesion complex. *Proc. Natl. Acad. Sci. USA.* 116:21545–21555.

58. Forero, M., O. Yakovenko, …, V. Vogel. 2006. Uncoiling mechanics of *Escherichia coli* type I fimbriae are optimized for catch bonds. *PLoS Biol.* 4:e298.

59. Vogel, V. 2018. Unraveling the mechanobiology of extracellular matrix. *Annu. Rev. Physiol.* 80:353–387.

60. Holle, A. W., X. Tang, …, A. J. Engler. 2013. In situ mechanotransduction via vinculin regulates stem cell differentiation. *Stem Cells.* 31:2467–2477.

61. Garakani, K., H. Shams, and M. R. K. Mofrad. 2017. Mechanosensitive conformation of vinculin regulates its binding to MAPK1. *Biophys. J.* 112:1885–1893.